═══REVIEW COMMONS MANUSCRIPT═══

IMPORTANT:

- Manuscripts submitted to Review Commons are peer reviewed in a journal-agnostic way.
- Upon transfer of the peer reviewed preprint to a journal, the referee reports will be available in full to the handling editor.
- The identity of the referees will NOT be communicated to the authors unless the reviewers choose to sign their report.
- The identity of the referee will be confidentially disclosed to any affiliate journals to which the manuscript is transferred.

GUIDELINES:

- For reviewers: https://www.reviewcommons.org/reviewers
- For authors: https://www.reviewcommons.org/authors

CONTACT:

The Review Commons office can be contacted directly at: office@reviewcommons.org

The role of stomatin-like protein (STOML) in *Plasmodium falciparum*

Julie M.J. Verhoef[1], Ezra T. Bekkering[1], Cas Boshoven[1], Megan Hannon[1], Nicholas I. Proellochs[1], Cornelia G. Spruijt[2], Taco W.A. Kooij[1]

[1]Department of Medical Microbiology, Radboudumc Center for Infectious Diseases, Radboud University Medical Center, Nijmegen, The Netherlands
[2]Department of Molecular Biology, Faculty of Science, Radboud University Nijmegen, Nijmegen, The Netherlands

*Corresponding author: Taco.Kooij@radboudumc.nl

Abstract

Members of the Stomatin, Prohibitin, Flotillin and HflK/C (SPFH) protein family form large membrane anchored or spanning complexes and are involved in various functions in different organelles. The human malaria causing parasite *Plasmodium falciparum* harbors four SPFH proteins, including prohibitin 1 and 2, prohibitin-like protein (PHBL), and stomatin-like protein (STOML) which all localize to the parasite mitochondrion. In the murine model parasite *Plasmodium berghei*, *STOML* has been shown to be essential and to localize to puncta on mitochondrial branching points in oocyst stages. In this study, we investigate the function of STOML in the human malaria parasite, *P. falciparum*. We show that deletion of *STOML* causes a significant growth defect and slower asexual blood-stage (ABS) development, while sexual-stage development remains unaffected. Parasites lacking *STOML* were not more sensitive to respiratory chain targeting drugs, rendering a function of STOML in respiratory chain assembly unlikely. Epitope tagging of endogenous STOML revealed a distinct punctate localization on branching points and endings of the ABS mitochondrial network. STOML resides in a large protein complex and pulldown experiments identified a zinc dependent metalloprotease, FtsH, as a likely interaction partner. The predicted AlphaFold structure of STOML shows high similarity with the bacterial HflK/C, which has been shown to form a large vault like structure around the bacterial FtsH hexamers. Combined, our results suggest that a similar STOML-FtsH complex localized to specific loci of *P. falciparum* mitochondria facilitate the parasite's asexual blood-stage development.

Introduction

Malaria is an infectious disease caused by *Plasmodium* parasites, which takes more than 600.000, mostly young lives annually[1]. *Plasmodium falciparum* is the most virulent malaria causing species. Resistance to current antimalaria drugs is fast to emerge, emphasizing the need for the continuous development of novel anti-malarial compounds. *Plasmodium* parasites harbor a unique mitochondrion that differs considerably from human mitochondria, which makes it a suitable drug target of antimalarial compounds such as atovaquone, DSM265, ELQ300, and proguanil[2,3].

The mitochondrion consists of an inner and outer membrane, which are both rich in large protein complexes. Indeed, the inner mitochondrial membrane (IMM) is considered one of the most protein-rich membranes in any cell-type and contains large multiprotein complexes, such as respiratory chain complexes, ATP synthase, and the mitochondrial contact site and cristae organizing system (MICOS). Similarly to all other biological membranes, the mitochondrial membranes are organized into domains of distinct protein and lipid composition[4,5]. These membrane microdomains are important for the spatial and temporal control of membrane protein complex assembly and regulation[4]. SPFH (Stomatin, Prohibitin, Flotillin and HflK/C) family proteins are enriched in eukaryotic and prokaryotic membrane microdomains of various organelles, such as plasma membrane, nucleus, endoplasmic reticulum (ER), and mitochondria[6]. The common feature of SPFH proteins is the presence of the highly conserved SPFH or Band-7 protein domain[7]. These proteins form large self-oligomerizing membrane-spanning or membrane-anchored complexes and have been indicated in a diverse set of functions[6]. A subset of SPFH proteins, including prohibitins (PHBs) and stomatin-like protein 2 (SLP2), localizes to the IMM. The two prohibitins (PHB1 and PHB2) form a large protein complex together, which has been indicated to play a role in mitochondrial protein degradation, cristae formation, mitochondrial dynamics, cell cycle regulation, and apoptosis[8–11]. SLP2 localizes to cardiolipin enriched membrane microdomains, where it interacts with and controls stability of the PHB complex[12,13]. The PHB and SLP2 complexes are both important for the formation and stability of the respiratory chain complex and mitochondrial translation[8,13–17]. They reside in large supercomplexes with metalloproteases and assert their proteolytic function through regulation of metalloprotease activity, similar to their bacterial family member HflIK/C[8,11,12,18–21].

Plasmodium parasites harbor three conserved SPFH proteins, including two prohibitins (PHB1 and PHB2) and stomatin-like protein (STOML), as well as an unusual myzozoan-specific prohibitin-like protein (PHBL)[22]. Attempts to delete the four genes using both genome-wide screens in *P. falciparum* and the murine malaria model parasite *Plasmodium berghei*, and targeted approaches in the latter, resulted in conflicting results with only *PHB2* consistently surfacing as essential. Localization studies through fluorescent tagging of the endogenous *P. berghei* genes revealed a mitochondrial localization of three SPFH proteins throughout the *P. berghei* life cycle[22]. Although tagging of *PHB1* was unsuccessful, PHB1/2 heterodimerization is evolutionary well-conserved[15,23] and *Pf*PHB1 ranks 84th on the validated list of *Plasmodium* mitochondrial proteins[24]. Functional complementation of yeast *PHB* mutants provided further support for prohibitin heterodimerization in *P. falciparum*[25]. *Pf*PHBs were shown to be involved in stabilizing mitochondrial DNA, maintaining mitochondrial integrity, and rescuing yeast cell growth[25]. PHBL-deficient parasites failed to

colonize *Anopheles* mosquitos as they arrest during ookinete development, which is correlated with depolarization of the mitochondrial membrane potential[22].

The role and importance of STOML remains unclear. Genetic screens in *P. falciparum* and *P. berghei* both suggested a dispensable role, yet targeted approaches did never yield a pure isogenic or clonal line free of wild-type parasites, indicating possible developmental issues. Interestingly, *Pb*STOML localizes to punctate foci at the parasite mitochondrion during oocyst growth, often at organellar branching points. This specific mitochondrial localization combined with the uncertainty about its importance and function drove us to further investigate the role of STOML in the human malaria causing *P. falciparum*.

In this study, we show that deletion of *STOML* in *P. falciparum* causes a significant growth delay of asexual blood stages (ABS), while sexual-stage development is not affected. *Pf*STOML localizes to punctate foci at mitochondrial branch endings and at branching points throughout ABS development. *Pf*STOML resides in a large protein complex and pulldown experiments identified metalloprotease FtsH as a likely interaction partner. We also show that the predicted AlphaFold structure of *Pf*STOML is highly similar to its bacterial family member HflK/C, which has recently been shown to form a large, oligomerized, vault structure around FtsH hexameres, this way regulating their accessibility. This suggests that a similar scenario might apply to the STOML-FtsH complex in *P. falciparum*. These results gave us novel insights into the function of STOML in *P. falciparum* and pave the way for future studies into the function of SPFH proteins and their potential as anti-malarial drug targets.

Results

Knockout of *PfSTOML* results in a significant growth defect

To study the function of *Pf*STOML (PF3D7_0318100) during ABS development, we aimed to generate *PfSTOML* knockout (KO) parasites using a targeted replacement strategy (Figure S1A). Although the first three transfection attempts were unsuccessful, we managed to generate two *PfSTOML* KO parasite lines in NF54 (*stoml*$^-$) and the MitoRed background (*stoml*$^-_{mito}$), which harbors a fluorescent mitochondrial marker (mito-mScarlet)[26]. Correct integration and the absence of unaltered wild-type (WT) NF54 or MitoRed parasite contaminations were verified by diagnostic PCR (Figure S1B). To demonstrate if *PfSTOML* KO causes a growth defect, we set up a new competition growth assay analogous to the protocol used with *Plasmodium berghei*[27]. In both *PfSTOML* KO lines, *stoml* is replaced by a *gfp* gene under the constitutive *P. falciparum* histone 2B (*Pf*H2B, PF3D7_1105100) promotor, making them green fluorescent. By mixing these with WT parasites harboring a constitutively expressed mScarlet, the relative abundance of red and green fluorescent parasites can be determined by flow cytometry and followed over time (Figure 1A). The average factor by which the red/green ratio changed from the first to the second timepoint in three independent experiments was defined as f_r. We included a control condition in which mNeonGreen expressing WT parasites (*cyto-NG*) are mixed with mScarlet expressing WT parasites (*cyto-mScarlet*) (Figure S2). We confirmed that the ratio of red and green parasites in this control culture was stable over time (f_r = 1.0) (Figure 1B). However, when co-culturing either of our *PfSTOML* KO lines with *cyto-mScarlet*, we found that the red/green distributions shift significantly over time (f_r = 20.9, $p<0.0001$). In one representative experiment, the ratio of *cyto-mScarlet* versus *stoml*$^-_{mito}$ parasites changes from 47 : 53, to 94 : 6 after one week and 99 : 1 after two weeks, indicating that *stoml*$^-_{mito}$ grows approximately 12 times slower in a week period compared to WT in mixed culture conditions. We observed a very similar trend in *stoml*$^-$ mixed cultures. To test whether this growth defect is caused by lower number of viable offspring per parasite, reduced invasion, or delayed development throughout the ABS cycle, we quantified growth and analyzed stage development microscopically in two independent experiments, either every 8-16 h over an 88-h period or daily for eight days (Figure 1C, 1D, 1E). These experiments showed that *stoml*$^-_{mito}$ develops slower throughout the ABS replication cycle compared to MitoRed WT parasites. At the end of the first replication cycle (40 h), MitoRed WT cultures contained mostly segmented schizonts and rings, and the parasitemia has increased 6.0-fold compared to the 24 h timepoint (Figure 1D). *stoml*$^-_{mito}$ cultures contained mostly early schizonts and very few rings at 40 h, and the parasitemia has only increased 1.6-fold. However, at 48 h, *stoml*$^-_{mito}$ parasitemia has almost "caught up" with WT parasitemia with a 4.9-fold increase compared to the 24 h timepoint. This trend of delayed ABS development continues in the next replication cycles (Figure 1E). These results indicate that *stoml*$^-_{mito}$ has a growth defect that is mostly caused by slower and prolonged development throughout the asexual replication cycle.

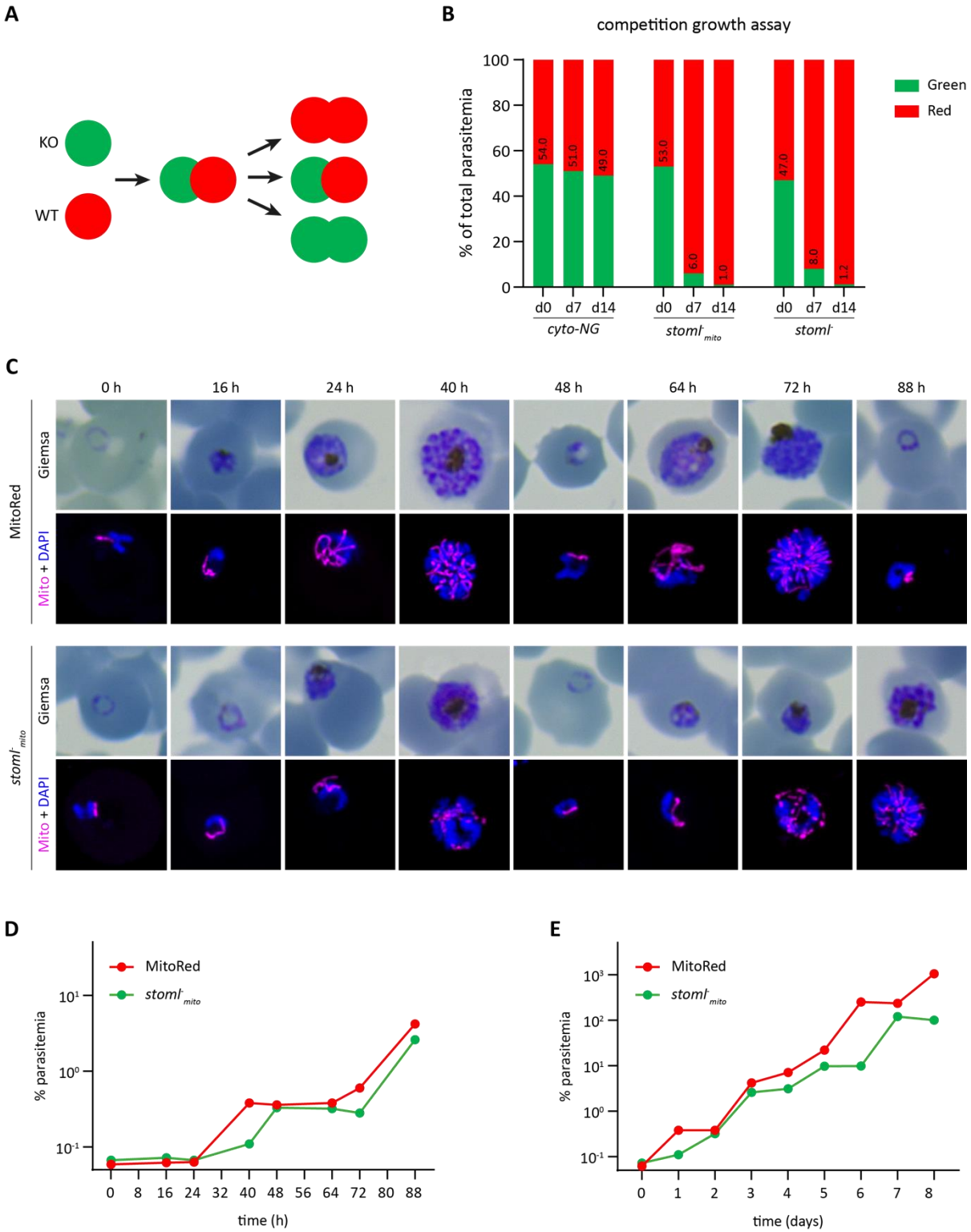

Figure 1. ABS development of* stoml$^{-}_{mito}$ *parasites is delayed. *A) Schematic overview of the competition growth assay.* PfSTOML *knockout parasites expressing cytosolic GFP (green) are mixed with wild-type parasites expressing cytosolic mScarlet (red) in an approximate 1:1 ratio. Overtime, the distribution of red/green parasites is measured using flow cytometry. If* PfSTOML *knockout causes a growth defect, the wild-type population will grow faster, and the ratio red/green parasites will shift. B) Bar graph showing distribution of red/green parasites in the competition growth assay at day 0, day 7 and day 14. The graph shows one representative example of three independent experiments.* Cyto-mScarlet *parasites are mixed with green* cyto-NG *(control),* stoml^{-}, *or* stoml$^{-}_{mito}$ *parasites to create mixed cultures. C) Giemsa-stained*

thin blood smears and fluorescent images showing the mitochondrial mScarlet marker (magenta) and DNA (blue) in MitoRed (WT) and stoml$^{-}_{mito}$ *parasites over time. Fluorescence microcopy images are maximum intensity projections of Z-stack confocal Airyscan images. D-E) Growth curve of parasitemia of MitoRed and* stoml$^{-}_{mito}$ *over time in hours (D) and days (E). In order to visualize continuous growth, we corrected for the parasitemia for the dilution factors, resulting in corrected parasitemias above 100%. The graphs show one representative experiments of two independent experiments.*

_Pf_STOML is unlikely to be involved in assembly of the respiratory chain

In other eukaryotes, STOML is thought to be involved in a variety of mitochondrial functions[13,21,28–30]. To explore if *Pf*STOML has a similar mitochondrial function in *P. falciparum*, we were curious to see if *PfSTOML* KO would alter mitochondrial dynamics. We compared mitochondrial morphology of *stoml*$^{-}_{mito}$ with MitoRed parasites and found no obvious differences throughout different stages of ABS development in two independent experiments (Figure S3). Mature *stoml*$^{-}_{mito}$ schizonts showed divided and segregated mitochondria, similarly to MitoRed WT parasites.

SLP2, the human STOML homolog, has been indicated to play an essential role in the assembly of the respiratory chain[12,28]. To test if STOML has a similar function in *P. falciparum*, we investigated if *stoml*$^{-}$ parasites would have an increased sensitivity to drugs targeting the respiratory chain. We performed drug assays with different mitochondrial drugs (including DSM1, DSM265, atovaquone, ELQ300 and proguanil) and non-mitochondrial drugs (chloroquine, DHA, MMV183) and found no difference in drug sensitivity between *stoml*$^{-}$ and WT parasites in two independent experiments (Figure S4). Energy metabolism in *P. falciparum* ABS relies heavily on glycolysis, and oxidative phosphorylation (OXPHOS) is only essential for ubiquinone recycling for pyrimidine synthesis[31]. However, in gametocytes, there is an increased TCA cycle utilization and presumably respiration[32,33]. We were therefore curious to see if *stoml*$^{-}_{mito}$ parasites could develop to mature gametocytes and gametes. We found that *stoml*$^{-}_{mito}$ parasites could develop to healthy-looking, mature gametocytes within a comparable time frame as WT parasites in three independent experiments. Mature male and female *stoml*$^{-}_{mito}$ gametocytes did not show obvious aberrations in mitochondrial morphology (Figure S5A). *Stoml*$^{-}_{mito}$ parasites were still able to exflagellate and had dispersed mitochondria after activation, similarly to what we have described for the MitoRed WT line[26] (Figure S5B). Based on these results, it is unlikely that STOML is directly involved in respiratory chain assembly in *P. falciparum*.

_Pf_STOML localizes to specific foci at the mitochondrion during ABS development

To learn more about the function of *Pf*STOML, we analyzed its subcellular localization. To do this, we generated a transgenic parasite line, *stoml-NG*, in which *STOML* is fused with a 3HA-mNG-GlmS tag. We also integrated a mitochondrial marker cassette mito-mScarlet for protein co-localization (Figure S1A). Correct integration and the absence of WT parasite contaminations were verified by diagnostic PCR (Figure S1B). Western blot analysis of ABS parasite extract confirmed expression of the full length *Pf*STOML-3HA-NG (Figure S1C). Live fluorescent microscopy of *stoml-NG* in three independent experiments showed localization of *Pf*STOML-3HA-NG to punctate foci during ABS development (Figure 2). In ring stages, *Pf*STOML-3HA-NG localized to a single spot, close to the mitochondrion (Figure 2A). As the parasites progress to late rings and the mitochondrion elongates, *Pf*STOML-3HA-NG is consistently found in two foci that reside at both endings of the mitochondrion (Figure 2A, 2B, Movie 1). In trophozoites, the mitochondrion starts to form a branched structure and

the number of *Pf*STOML-3HA-NG foci per parasite increases (Figure 2C). *Pf*STOML-3HA-NG foci are found both at endings of mitochondrial branches, as well as branching points (Figure 2A). Similar localization is found in early schizont stages, were the mitochondrion forms a complex, branched network (Figure 2A, 2B, Movie 2). The number of foci per parasite increases during schizont stages. In late schizonts, when the mitochondrial branches orient in a radial fashion prior to division, the *Pf*STOML-3HA-NG foci are found at the endings of most mitochondrial branches, although *Pf*STOML-3HA-NG signal can also be observed along mitochondrial branches (Figure 2A, 2B, Movie 3). In a fully segmented parasite that seems to have egressed form the RBC, only few *Pf*STOML-3HA-NG foci were found. This unique localization pattern is different from the homogeneous mitochondrial localization of *Pb*STOML observed in *P. berghei* ABS[22].

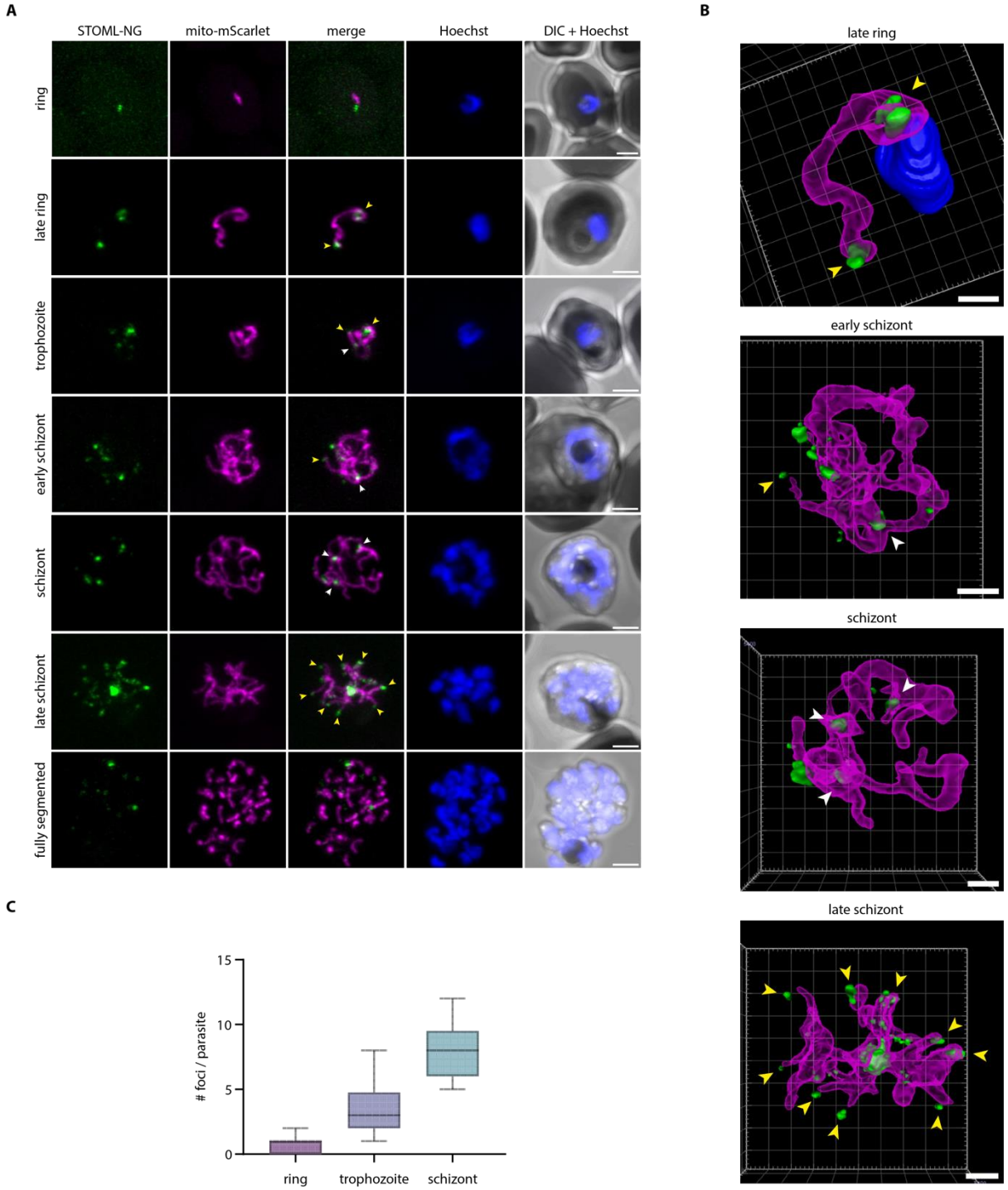

Figure 2. Localization of STOML-3HA-NG in ABS parasites. *A) Live imaging of* stoml-NG *with* Pf*STOML-3HA-NG (green), mito-mScarlet mitochondrial marker (magenta), Hoechst for DNA visualization (blue) and DIC through the asexual replication cycle. Images are maximum intensity projections of Z-stack confocal Airyscan images. Arrowheads indicate* Pf*STOML-3HA-NG signal at mitochondrial branching points (white) or mitochondrial branch endings (yellow). Scale bars, 2 μm. B) 3D visualization of Z-stack confocal Airyscan images using Arivis 4D vision software. Fluorescent signal is segmented by manual thresholding. Arrowheads indicate STOML-NG signal at mitochondrial branching points (white) or mitochondrial branch endings (yellow). Scale bars, 1 μm. C) Boxplot indicating number of* Pf*STOML-3HA-NG foci per parasite in ring (n=7), trophozoite (n=12) and schizont (n=9) stages with a total of 28 parasites.*

_Pf_STOML resides in a large protein complex with _Pf_FtsH

PHBs and STOML are found in large hetero- and homo- oligomers at the IMM in other eukaryotes, such as humans and yeast[15,21]. *P. falciparum* mitochondrial complexome profiling data showed that *Pf*STOML migrates in a large ~2 MDa protein complex on a native gel (Figure 4C)[33]. In order to identify the proteins in this complex, we performed two independent pulldown experiments (Figure 4A-B, S6). In the first experiment, late-stage *stoml-NG* parasites (24-40 h.p.i.) were lysed through saponin lysis and nitrogen cavitation, and organelle fraction was used as input for co-immunoprecipitation with anti-mNG coated magnetic beads. As a control, the same fraction was loaded on uncoated beads. Mass spectrometry revealed that 27 proteins were significantly enriched after pulldown with mNG beads, of which *Pf*STOML was the most significantly enriched (Figure 4A, Table S2). For the second pulldown experiment, we generated a transgenic parasite line in which *STOML* is fused with an 3HA-GlmS tag, which we termed *stoml-HA*. Correct integration and the absence of wild-type (WT) parasite contaminations were verified by diagnostic PCR (Figure S1B) and Western blot analysis confirmed expression of STOML-3HA (Figure S1C). Organelle fraction of late-stage *stoml-HA* parasites was used as input for pulldown with anti-HA coated magnetic beads and empty protein G beads were used as control. In the second experiment, 122 proteins were significantly enriched after HA pulldown (Figure S6, Table S3). Three proteins were significant hits in both pulldown experiments: STOML, an ATP-dependent zinc metalloprotease FtsH (PF3D7_1464900), and a conserved protein of unknown function (PF3D7_1306200) (Figure 4B). Although FtsH is also found in a large protein complex of ~2.5 MDa in the complexomics dataset[33], it does not perfectly comigrate with the STOML complex in ABS (Figure 4C). In gametocytes, however, FtsH and STOML comigrate at ~2.3 MDa. In contrast, PF3D7_1306200 does not comigrate with STOML in either ABS or gametocyte stages. PF3D7_1306200 is predicted to be an essential protein and is expressed in late schizonts[34,35]. It contains an AB-hydrolase domain and is thought to localize to the apicoplast. FtsH, on the other hand, is a predicted mitochondrial protein (ranking 265th with a mitochondrial prediction score of 2.1[24]) and phylogenetic analysis shows clustering with *i*-AAA proteases in the IMM[36].

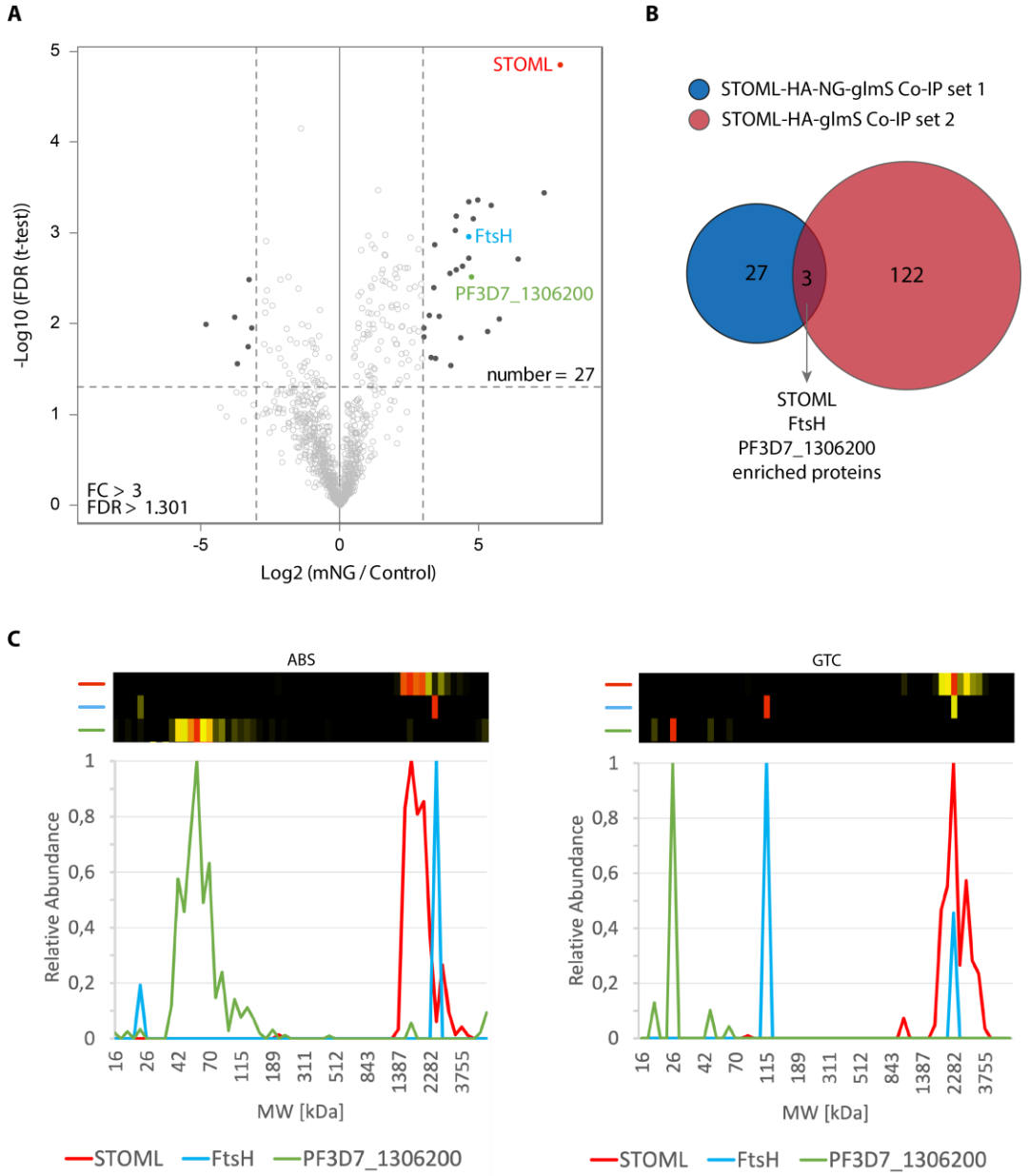

Figure 4. Identification and characterization of STOML protein complex. *A) Anti-mNG co-immunoprecipitation of* Pf*STOML-3HA-mNG containing complexes. The volcano plot showing mean log_2 fold changes (FC) and -log_{10} false discovery rate (FDR) for anti-HA pulldown in comparison with control pulldown. Horizontal and vertical dotted lines indicate FC > 3 and FDR > 1.301 respectively. Dark dots represent proteins that are highly enriched in the anti-mNG pulldown compared to the control pulldown. B) Overlap of enriched proteins in both anti-HA pulldown on STOML-HA and anti-NG pulldown on STOML-NG. C) Heatmap and graph showing migration profiles of STOML (red), FtsH (blue) and PF3D7_1306200 (green) on a blue native gel with a normalized relative abundance of 1 (red) represents the highest iBAQ value for a given protein and the molecular weight (MW) indicated on the x-axis.*

SPFH proteins are known to form large protein complexes with metalloproteases, regulating their protease activity[8,18,19,21,37]. The human STOML homolog, SLP2, forms a large proteolytic complex termed the SPY complex at the inner mitochondrial membrane with rhomboid protease PARL and *i*-AAA metalloprotease YME1L[21]. SLP2 regulates the activity of YME1L, which forms homo-hexamers and is involved in degradation of unfolded or excess mitochondrial proteins[38]. In *Trypanosoma brucei*, another unicellular protozoan parasite,

SLP2 can also be found in a complex with the Yme1L homolog, *Tb*Yme1[39]. A BLAST search of *h*YME1L identified *P. falciparum* FtsH as top hit with 41% identity (Figure S7).

Cryo-electron microscopy revealed that the bacterial HflK and HflC form a large, hetero-oligomeric vault structure around four membrane-anchored FtsH hexamers (Figure 5E)[19]. We compared the predicted AlphaFold[40] structure of *Pf*STOML with the bacterial HflK/C complex (Figure 5A-D). Although *Pf*STOML lacks a clear transmembrane domain, the overall predicted structure of the protein is highly similar to its bacterial family members. To further explore if *Pf*STOML could form a similar multimer barrel structure, we used AlphaFold multimer[41] to predict the *Pf*STOML 24-multimer structure (Figure S8A). We used the SPFH2 and long alpha helix domains of *Pf*STOML, as these are the best predicted parts of the *Pf*STOML structure (pLDDT>90). The *Pf*STOML 24-multimer structure was predicted to form a round, yet distorted barrel structure with the endings of the multimer structure not joining together to close the structure, which visually seemed to include too many *Pf*STOML proteins (Figure S8A). In order to estimate the correct amount of *Pf*STOML proteins in the barrel complex, we used AlphaFold multimer to predict the structure of *Pf*STOML 8-multimer structure with SPFH1, SPFH2 and long alpha helix domains (Figure S8B). We then measured the angle between the SPFH domains in the 8-multimer complex to estimate the curvature of the barrel (Figure 8SC). We found an angle of 16.5 degrees between SPFH domains, suggesting that the *Pf*STOML complex might consist of approximately 22 *Pf*STOML monomers. Indeed, AlphaFold predicts an intact, slightly oval barrel structure for a *Pf*STOML 22-multimer with SPFH2 and long alpha helix domains (Figure 5F, S8D). The predicted *Pf*STOML 22-multimer structure showed high similarity with the HflK/C-FtsH complex, indicating that STOML might form a similar supercomplex with FtsH in the IMM in *P. falciparum*.

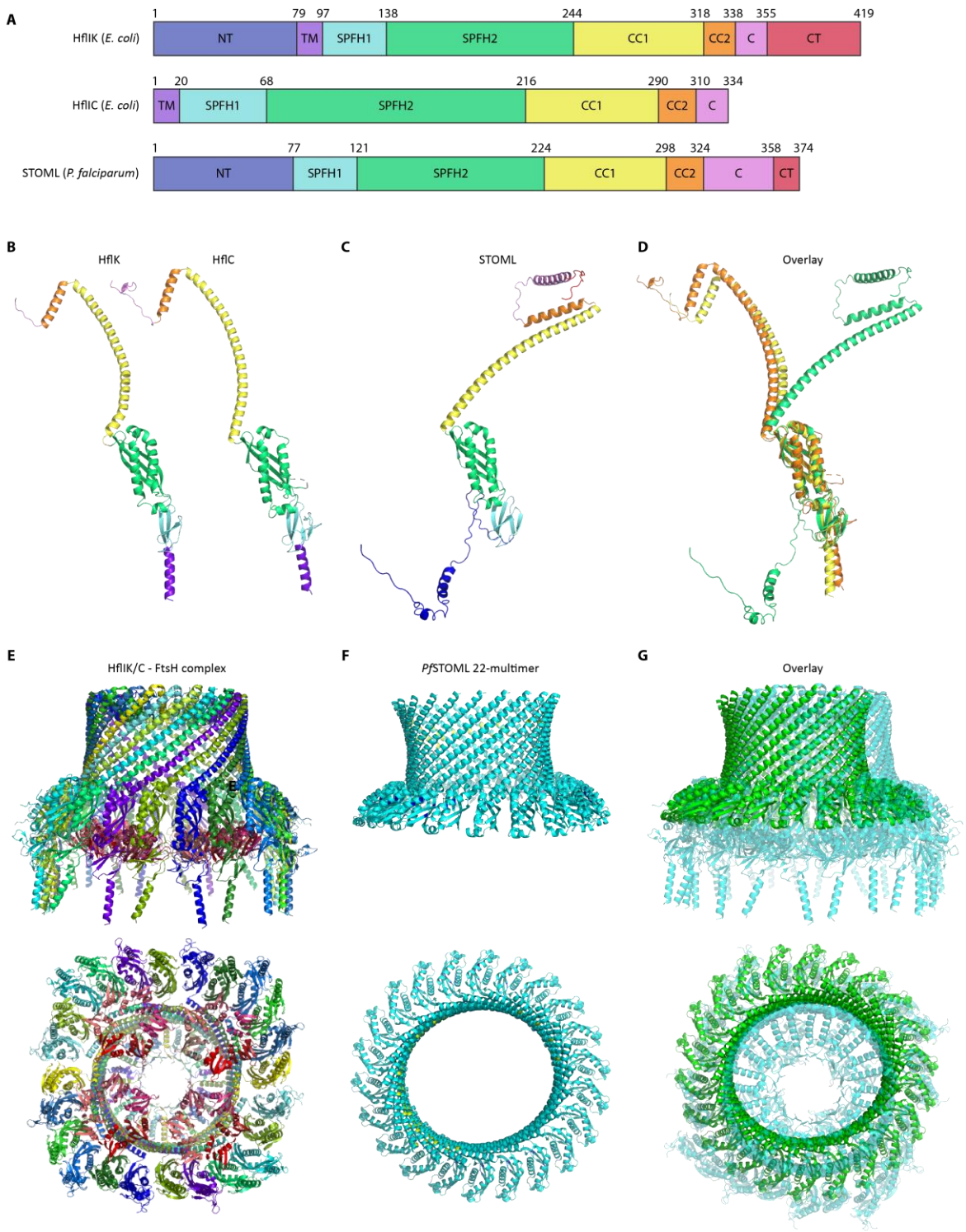

Figure 5. AlphaFold predictions of* Pf*STOML complex structure and comparison with the bacterial HflK/C supercomplex structures. *A) Protein domains of* Ec*HflK* Ec*HflC, and* Pf*STOML, indicated are transmembrane domain (TM), SPFH1 and SPHF2 domains, long coiled-coil domain 1 (CC1), coiled-coil domain 2 (CC2), C-terminal region (CT). B) Protein structures of* Ec*HflK and* Ec*HflC* determined by *Ma* et al.[19]. *C) Predicted AlphaFold structure of* Pf*STOML. D) Overlay of* Ec*HflK and* Ec*HflC structures with* Pf*STOML AlphaFold structure. E) Cryo-EM structure of HflK/C – FtsH complex with the side view (top) and bottom view (bottom). Purple/blue-colored proteins are HflC, green/yellow-colored proteins are HflK, red/pink-colored proteins are part of the FtsH hexamers. F) Predicted AlphaFold structure of* Pf*STOML 22-multimer with side view (top) and top view (bottom), coloring according to model confidence with very high confidence (pLDDT > 90) dark blue, high confidence (pLDDT > 70) light blue, and low confidence*

(pLDDT > 50) yellow. G) Overlay of predicted AlphaFold Pf*STOML 22-multimer structure (green) with HflK/C – FthsH complex (light blue) with side view (top) and top view (bottom).*

Discussion

The SPFH protein family is a highly conserved family involved in the formation of microdomains in membranes of various organelles. Prohibitins and stomatin-like protein (STOML) are localized to the IMM and have been implicated in several mitochondrial functions, including cristae formation and assembly of the respiratory chain[11,12,14,28]. *Plasmodium* harbors four SPFH family members, including two prohibitins (PHB1 and PHB2), a prohibitin-like protein (PHBL), and STOML, which localize to the mitochondrion[22]. STOML is likely essential in *P. berghei* and localizes to foci on mitochondrial branching points during oocyst stages. In this study, we investigated the function of STOML in the human malaria causing parasite *P. falciparum*.

In contrast to the *in vivo* murine model parasite *P. berghei* in which *STOML* could not be deleted, we were able to generate two *STOML* KO lines in *P. falciparum*. *stomlˉ* parasites developed slower throughout the ABS replication cycle compared to WT parasites, indicating an important but non-essential function for *PfSTOML* under *in vitro* culture conditions. In trophozoite and schizont stages, *Pf*STOML localizes to specific foci at the mitochondrial branching points and endings of mitochondrial branches. In late schizonts, when mitochondrial branches are oriented in a radial fashion prior to division[26], *Pf*STOML has a punctate localization at the endings of mitochondrial branches. While STOML appears to have a more uniform mitochondrial distribution in most *P. berghei* life cycle stages, *Pb*STOML localizes to foci on mitochondrial branching points in oocyst stages[22]. This specific localization suggests a potential function for *Pf*STOML in mitochondrial dynamics and/or segregation. This could explain why *PfSTOML* deletion did not affect the sexual stage development, during which parasites do not undergo cell division. On the other hand, *PfSTOML* knockout does not seem to affect mitochondrial division, and segregation (Figure S3). Therefore, the exact function of *Pf*STOML at this specific mitochondrial localization remains to be elucidated.

In human, yeast and plants, STOML has been indicated to play a role in the assembly of the respiratory chain[12,13,28]. We hypothesized that STOML might have a similar function in *P. falciparum* and that *PfSTOML* knockout would lead to an increased sensitivity to drugs targeting the respiratory chain, such as atovaquone and ELQ300. However, our data show no changes in drug sensitivity upon *PfSTOML* knockout. Additionally, $stomlˉ_{mito}$ parasites were able to form healthy gametocytes and undergo male gametogenesis, during which mitochondrial ATP synthesis is thought to be essential[42]. This indicates that in contrast with orthologs in other eukaryotes, *Pf*STOML is not directly involved in respiratory chain assembly in *P. falciparum*.

Our mitochondrial complexomics data shows that *Pf*STOML consistently resides in a large ~2 MDa protein complex[33]. SPFH proteins are known to form large homo- or heteromeric complexes, often together with proteases[8,18]. In order to further characterize the STOML complex in *P. falciparum*, we performed two complementary STOML-pulldown experiments to identify potential interactors. Three proteins, including *Pf*STOML, *Pf*FtsH metalloprotease, and a protein of unknown function (PF3D7_1306200), were identified as significantly

enriched in both pulldown experiments. PF3D7_1306200 contains an AB-hydrolase domain and is predicted to be essential[34]. Similarly to STOML, it is mostly expressed in schizont stages[35], yet the putative hydrolase is predicted to localize to the apicoplast[43] and did not show comigration with STOML on a native gel in our complexomics data[33]. Based on its predicted apicoplast localization, and the lack of comigration with *Pf*STOML on a native gel, it is unlikely that PF3D7_1306200 forms a complex with *Pf*STOML at the IMM, yet, the consistent pull down with the STOML-FtsH complex is remarkable. Particularly in the light of a recent discovery of an AB-hydrolase, ABHD16A, localized to the endoplasmic reticulum in human cell lines, that appears to regulate the recruitment of fission and fusion machineries to mitochondria by altering phospholipid composition at ER-mitochondria membrane contact sites[44].

*Pf*FtsH belongs to the AAA (ATPases Associated with various cellular Activities) metalloprotease family at the IMM, which play a role in protein surveillance by degrading non-native integral membrane proteins and membrane associated proteins such as unassembled units of the respiratory chain[45,46]. *P. falciparum* harbors three FtsH homologs[36]. Two of the *P. falciparum* FtsH homologs, including PF3D7_1464900, which we identified in our STOML pull-down, locate to the IMM, have a single transmembrane domain, and cluster with *i*-AAA FtsH homologs, which are exposed to the intermembrane space. The third homolog, *Pf*FtsH1 (PF3D7_1239700), has two transmembrane domains and clusters with *m*-AAA FtsH homologs at the IMM that are exposed to the mitochondrial matrix. *Pf*FtsH1 forms oligomeric complexes and has a punctate distribution on the mitochondrial branching points in late trophozoite and early schizont stages[36], which is similar to STOML distribution in these stages. Contradictory, another study showed that actinonin, a small molecule inhibitor, targets *Pf*FtsH1 and disrupts apicoplast biogenesis[47] and its homolog in *T. gondii* is also localized to the apicoplast[48]. Expression of *Pf*FtsH1 in *E. coli* causes defective cytokinesis, implying a potential role in organelle division. Unfortunately, Amberg-Johnsen and colleagues were unable to generate endogenously tagged knockdown parasite lines of the two *i*-AAA proteases[47]. Therefore, the exact function and substrates of FtsH in *P. falciparum* remains to be elucidated.

The interaction between STOML and PfFtsH is well-supported by evidence. Their respective human homologs, SLP2 and Yme1L, form the SPY complex[21], which is essential for the proteolytic regulation of proteins involved in mitochondrial dynamics and quality control. Yme1L also contributes to OPA1 cleavage, a mitochondrial GTPase which is involved in mitochondrial fusion and cristae formation[49,50], however, no *Plasmodium* OPA1 homolog has been identified to date. In *Trypanosoma brucei*, *Tb*SLP2 forms a large mitochondrial complex with *Tb*Yme1, which is involved in mitochondrial stress resistance[39]. Also in filamentous fungus *Neurospora crassa*, STOML2 has been found in a large complex with an *i*-AAA protease (IAP1)[51]. Furthermore, other SPFH family members are known to form large complexes with AAA+ proteases, such prohibitins with Yta10/Yta12 in yeast[8] or HflK/C with FtsH in bacteria[18]. Characterization of the HflK/C-FtsH supercomplex structure showed that HflK/C forms a 24-heteromer vault structure around four hexameric FtsH complexes at the bacterial membrane[52] (Figure 5E). Here, we show that the *Pf*STOML AlphaFold predicted structure shows high similarity with that of bacterial HflK/C. Our AlphaFold multimer predictions indicate it is likely that *Pf*STOML forms a 22-multimer barrel structure that is highly similar to the vault structure of HflK/C-FtsH supercomplex in bacteria. Although these

predictions are based on modelling and therefore need to be interpreted with caution, the high structural similarity of the *Pf*STOML 22-multimer complex with HflK/C-FtsH supercomplex, combined with our co-immunoprecipitation data, suggests that *Pf*STOML might form a similar supercomplex structure with *Pf*FtsH, possibly regulating *Pf*FtsH accessibility.

Taken together, we have demonstrated that KO of *PfSTOML* causes a significant delayed ABS development, while gametocytes develop normally. *Pf*STOML has a punctate distribution to mitochondrial branching points and endings of mitochondrial branches, but knockout of *PfSTOML* does not affect mitochondrial morphology. Knockout of *PfSTOML* did not affect sensitivity to drugs targeting the respiratory chain, suggesting that *Pf*STOML is not directly involved in respiratory chain assembly. *Pf*STOML resides in a large supercomplex with *Pf*FtsH, likely forming a large, multimeric barrel structure that regulates the accessibility of *Pf*FtsH, similar to its bacterial family members. Although the exact function of the STOML-FtsH complex in *P. falciparum* remains to be elucidated, these results could pave the way for future studies into this highly conserved protein family and their role in proteolytic processes and membrane organization.

Materials and Methods

P. falciparum culture and transfections

P. falciparum NF54 and mutant parasites lines were cultured in RPMI1640 medium supplemented with 25 mM HEPES, 10% human type A serum (Sanquin, The Netherlands) and 25 mM $NaHCO_3$ (complete medium). Parasites were cultured in 5% human RBCs type O (Sanquin, The Netherlands) at 37°C with 3% O_2 and 4% CO_2. For transfection, 60 µg of HDR plasmid was linearized by overnight digestion, precipitated, and transfected with 60 µg Cas9 plasmid using either RBC loading or ring transfection[53]. For RBC loading, plasmids were loaded into RBCs by electroporation (310 V, 950 µF) and a trophozoite parasite culture was added to the transfected RBCs. One day after transfection, parasites were treated with 2.5 nM WR99210 (Jacobus Pharmaceutical) for five days. For ring transfection, a ring-stage sorbitol synchronized parasite culture was transfected with the plasmids by electroporation (310 V, 950 µF). Five hours after transfection, parasites were treated with 2.5 nM WR99210 for five days. Success of transfection was assessed by diagnostic PCR (Figure S1). Gametocyte cultures were maintained in a semi-automatic culturing system with media changes twice a day[54]. Gametocytes were stress-induced through asexual overgrowing. A mixed asexual culture of 1% was set up and cultured for up to 2 weeks.

Plasmid constructs

To generate *STOML* KO repair plasmid, pGK plasmid was used, which contains a pBAT backbone with H2B promotor, GFP and PBANKA_142660 bidirectional 3'UTR, flanked by multiple cloning sites. 5' and 3' Homology Regions (HRs) were amplified and cloned into pGK sequentially, using XmaI + XhoI and NcoI + EcoRI restriction sites respectively, generating pRF0038 *STOML* KO repair plasmid. CRISPR-Cas9 guide plasmids targeting two different sites in *STOML* were generated. Guide oligonucleotides were annealed and cloned into pMLB626 plasmid (a kind gift from Marcus Lee) using BbsI restriction enzyme, generating the pRF0039 and pRF0040 final guide plasmids (Table S1).

To generate *STOML* tagging repair plasmid, pRF0079 empty tagging plasmid was used, containing 3HA-NG-GlmS, PBANKA_142660 bidirectional 3'UTR, and the mito-mScarlet mitochondrial marker[26]. 5' HR was generated by overlap PCR, harboring a shield mutation that prevents cutting of CRISPR-Cas9 when the construct is integrated. 5' and 3' HRs were cloned into pRF0079 using KpnI + BamHI and EcoRI + NgoMIV restriction enzymes respectively, generating pRF0166 *STOML* tagging plasmid. Because this plasmid was unsuccessful in generating mutant parasite line after three transfection attempts, we decided to clone the *DHFR* selection marker in the repair plasmid and remove it from the guide plasmid. By addition of WR after transfection, we will then directly select for parasites with integration of the *DHFR* cassette, instead of selection on the guide plasmid. The *DHFR* cassette was removed from pRF0040 guide plasmid by digestion with EcoRI and ApaI, followed by blunt end generation with DNA polymerase I (klenow), following manufacturer's instructions, and ligation. The new guide plasmid without *DHFR* was termed pRF0210. The *DHFR* cassette cloned from MLB626 plasmid into pRF0166 with SphI and EcoRI restriction enzymes, generating pRF0213 3HA-NG-GlmS tagging plasmid with mito-mScarlet and *DHFR* selection marker. Since a big fluorescent tag might interfere with protein function, we also generated a *STOML* tagging repair plasmid by removing mNG from pRF0213, generating pRF0266 3HA-GlmS tagging plasmid, using BamHI and NheI restriction enzymes.

For generation of the repair plasmids for cyto-mScarlet and cyto-mNG parasite lines (used for the competition growth assay), SIL7 reporter plasmid (pRF0057) was used[26]. *mScarlet* gene was amplified from p1.2RhopH3-HA-mScarlet (a kind gift from Prof. Alan Cowman) (Table S1) and cloned into pRF0057 using AfeI and NheI restriction enzymes, generating pRF0278 cyto-mScarlet repair plasmid. *mNeonGreen* was amplified from pRF0079 plasmid and cloned into pRF0278 with AflII and NheI restriction sites to generate pRF0290, the cyto-mNG repair plasmid. CRISPR-Cas9 guide plasmids targeting SIL7 were used[26]. All enzymes used were obtained via New England Biolabs.

Competition growth assay

For the competition growth assay, parasite lines harboring a cytosolic mScarlet or cytosolic mNG were generated by integration of cyto-mScarlet and cyto-mNG constructs in SIL7 integration site[26]. Cyto-

485 mScarlet, Cyto-mNG, *stomI⁻* and *stomI⁻$_{mito}$* were synchronized by a 63% Percoll centrifugation. Late-stage
486 parasites were isolated from the Percoll gradient and added to fresh RBCs. Four hours later, 5% sorbitol
487 synchronization was performed, which allowed only young rings that just invaded a new RBC to survive.
488 Ring-stage parasites were counted and diluted to each have 0.4% final parasitemia in Cyto-mScarlet +
489 Cyto-mNG, Cyto-mScarlet + *stomI⁻,* and Cyto-mScarlet + *stomI⁻$_{mito}$* mixed cultures. Samples for flow
490 cytometry analysis were taken directly after set-up, at day 7 and at day 14. Samples from each mixed
491 culture were taken and stained with 0.5 µg/ml Hoechst 33342 (Invitrogen, H3570) for 30 min at 37°C.
492 Samples were directly analyzed on BD FACSAria™ III Cell Sorter and number of red and green parasites
493 were counted. Data was analyzed in FlowJo (version 10.10).
494
495 **Growth assay**
496 For this growth assay, MitoRed (WT), *stomI⁻*, and *stomI⁻$_{mito}$* parasites were synchronized by a 63% Percoll
497 centrifugation. Late-stage parasites were isolated from the Percoll gradient and added to fresh RBCs.
498 Four hours later, 5% sorbitol synchronization was performed, which allowed only young rings that just
499 invaded a new RBC to survive. Ring-stage parasites were counted and diluted to 0.05% parasitemia.
500 Samples for flow cytometry analysis and fluorescent microscopy were taken directly after setup (t=0),
501 and then every 8, 16 or 24 h over a period of 8 days. To prevent overgrowth, parasite cultures were cut
502 back 1/100 on day 3, and 1/50 on day 6. For flow cytometry, samples were taken and fixed in 0.25%
503 glutaraldehyde. All samples from different time points were processed at the same time, by staining with
504 Hoechst 33342 for 30 min at 37°C and then analyzed by flow cytometry (Beckman Coulter Cytoflex) to
505 determine parasitemia using the 405 nm laser. Data was analyzed in FlowJo (version 10.10). Final
506 parasitemia was adjusted for the dilution factor, explaining why final parasitemia can reach more than
507 100%. For fluorescent microscopy, parasite samples were processed as described in "fixed imaging"
508 paragraph below.
509
510 **Live imaging**
511 *StomI-NG* parasites were stained with Hoechst 33342 for 30 min at 37°C and settled in an 8-well imaging
512 chamber (Ibidi) in complete media without phenol red. Parasites were imaged on a Zeiss LSM880 or
513 LSM900 Airyscan microscope with 63x oil objective and 37°C heated stage, using 405, 488, and 561 nm
514 excitation lasers. Images were Airyscan processed before analysis with FIJI software.
515
516 **Fixed imaging**
517 Fluorescent microscopy was performed on asexual and sexual blood-stage *stomI⁻$_{mito}$* parasites, using the
518 same fixation and staining protocols. Parasites were settled on a poly-L-lysine coated coverslip for 20 min
519 at 37°C. Parasites were fixed (4% EM-grade paraformaldehyde, 0.0075% EM-grade glutaraldehyde in PBS)
520 for 20 min and permeabilized with 0.1% Triton X-100 for 10 min. DNA was visualized by staining with 1
521 µM DAPI in PBS for 1 h. PBS washes were performed between different steps. Parasites were mounted
522 with Vectashield (Vector Laboratories). Samples were imaged with Zeiss LSM880 or LSM900 Airyscan
523 microscope with 63x oil objective and 405, 488, and 561 nm excitation lasers. Images were Airyscan
524 processed before analysis with FIJI software.
525
526 **Co-immunoprecipitation assay**
527 *StomI-HA* and *stomI-NG* parasites were synchronized with 5% sorbitol and harvested 22 h later to obtain
528 late-stage parasites. Parasites were treated with 0.06% saponin, snap-frozen in liquid nitrogen, and
529 stored at -80°C until further processed. Nitrogen cavitation was used for cell disruption as described[33].
530 On the day of the experiment, 18 pellets of 30-ml cultures per parasite line were resuspended and pooled
531 in 25 ml ice-cold MESH-buffer (250 mM sucrose, 10 mM HEPES, 1 mM EDTA, 1× cOmplete™ EDTA-free
532 Protease Inhibitor Cocktail (Sigma), pH 7.4). The sample was added to the pre-chilled cell disruption
533 vessel (#4639 Parr Instrument Company) and pressurized with nitrogen gas at 1500 psi for 45 min on ice.
534 The parasites were then sheared through slow release. The organelle-enriched fraction was obtained by
535 differential centrifugation as described[33]. Protein concentrations were determined by Pierce™ BCA
536 Protein Assay Kit (Thermo Scientific). Samples were solubilized with n-dodecyl-β-D-maltoside (DDM)
537 (Sigma), using 3:1 detergent:protein (w/w) ratios. Solubilized samples were spun down at 22,000 x g at
538 4°C. Supernatant derived from *stomI-NG* samples were applied on ChromoTek mNeonGreen-Trap

magnetic agarose beads (ChromoTek), or empty control agarose beads (ChromoTek). Supernatant from *stoml-HA* samples were applied on Pierce™ HA-tag magnetic beads (Thermofisher) or empty protein G control beads (Thermofisher). Beads were incubated at 4°C for 30 minutes with gentle agitation and then washed twice with washing buffer (PBS, 1mM EDTA, 1× cOmplete™ EDTA-free Protease Inhibitor Cocktail, 0.05% DDM) and three times with ice-cold PBS, using a magnetic stand. After washes, on bead digestion was performed as follows: beads were resuspended in 50 µl elution buffer (2M urea, 100 mM Tris-HCl pH 8.0, 10 mM DTT) and incubated for 20 minutes at 25°C while shaking. To alkylate cysteines, iodoacetamide was added to a final concentration of 50 mM. Samples were kept in the dark for 10 min at 25°C. Subsequently, 0.25 µg of sequencing grade tryspin (Promega) was added to digest the proteins. The samples were shaken at 25°C for 2 h. The supernatants, containing the partially digested proteins, were collected and 50 µl of fresh elution buffer was added to the beads and shaken for another 5 min. Next, these supernatants were collected and combined with the first supernatant. Another 0.1 µg of trypsin was added, to stimulate overnight digestion at 25°C. The next day, samples were concentrated and purified on C18 stagetips[55]. Samples were analyzed on a Thermo Exploris 480 mass spectrometer, operated with an online Easy-nLC 1000. A gradient of buffer B (80% acetonitrile, 0.1% formic acid) was applied for 60 min. The mass spectrometer was ran in Top20 mode, while dynamic exclusion was enabled for 45 sec. Raw data was analyzed using Maxquant version 1.6.6.0[56] with a *Plasmodium* database (strain 3D7, version August 5th 2022, obtained from plasmodb.org[57]). LFQ, iBAQ and match between runs were enabled, and deamidation (NQ) was added as additional variable modification. The output was filtered using Perseus 1.5.0.15[58]. Proteins marked as potential contaminants, reverse hits, and proteins with less than 2 peptides were removed. Samples were grouped into triplicates, and proteins with less than 3 valid values in at least 1 group were removed, after which missing values were imputed using the default settings. A t-test was performed to identify specific outliers. Data was visualized using R.

Drug sensitivity assay

NF54 and *stoml*$^{-}$ parasites were used in a replication assay as described[59] to determine sensitivity to anti-malarial compounds. Briefly, parasites were diluted to 0.83% parasitemia and 3% hematocrit. Thirty microliters of diluted parasites were combined with 30 µl of compound serially diluted in dimethyl sulfoxide (DMSO) and RPMI 1640 medium to reach a final DMSO concentration of 0.1% in a total assay volume of 60 µl. Parasites were incubated at 37°C for 72 hours with mixed gas (3% O_2 and 4% CO_2). Then 30 µl of lysis buffer containing 1:15,000 SYBR Green reagent (Life Technologies), 13.3 mM Tris-HCl, 3.3 mM EDTA, 0.067% TritonX-100 and 0.0053% saponin was added and fluorescence intensity was quantified using BioTek Synergy 2 plate reader. GraphPad Prism was used for data analysis and inhibitory dose-response curves were determined with a variable slope model, in which the curve is generated with the following formula: $y = Bottom + (Top - Bottom)/(1 + 10^{(logIC50-x)*Hillslope})$.

DALI search and AlphaFold structure predictions

To identify proteins with similar structure, the *Pf*FtsH AlphaFold[40] structure (accessed 12 April 2024) was submitted to a DALI PDB search available through the web application (http://ekhidna2.biocenter.helsinki.f/dali/) using "matches against PDB90" result section. AlphaFold multimer[41] predictions were performed using the COSMIC[2] platform (https://cosmic-cryoem.org/tools/alphafoldmultimer/). All (predicted) protein and protein complex structures and alignments were visualized using PyMOL Molecular Graphics System (version 2.5.2. Schrödinger, LLC).

Acknowledgements

We are very grateful to Prof. Akhil Vaidya for the insightful discussions. We would like to thank all members of the molecular & cellular parasitology team at Radboudumc for the insightful discussions. We would like to thank the Radboud Technology Center Microscopy for use of their microscopy facilities. We also thank the Radboud Technology Center Flowcytometry for the use of their flowcytometry facilities. We are grateful to Koen Dechering and Tonnie Huijs for their support with the drug sensitivity assays. We thank Marcus Lee for providing the pMLB626 CRISPR/Cas9 guide plasmid. J.M.J.V. and E.B. are

supported by individual Radboudumc Master-PhD grants, C.B. by a PhD fellowship from the Radboud Institute for Molecular Life Sciences, Radboudumc (RIMLS018-009b).

Author Contributions

JV and TK designed the study. JV, CB, MH, and NP generated transgenic parasite lines. JV and EB conceived and performed experiments. CB and MH developed the competition growth assay. CS performed the mass spectrometry experiments and data analysis. J.V wrote the first draft of the manuscript. EB and TK edited the manuscript. TK supervised the project. All authors read and approved of the manuscript.

References

1. WHO. *World malaria report 2023*. (2023).
2. Lamb, I. M., Okoye, I. C., Mather, M. W. & Vaidya, A. B. Unique Properties of Apicomplexan Mitochondria. *Annu. Rev. Microbiol.* **77**, 541–560 (2023).
3. Goodman, C. D., Buchanan, H. D. & McFadden, G. I. Is the mitochondrion a good malaria drug target? *Trends Parasitol.* **33**, 185–193 (2017).
4. Laude, A. J. & Prior, I. A. Plasma membrane microdomains: Organization, function and trafficking (Review). *Mol. Membr. Biol.* **21**, 193–205 (2004).
5. Whitelegge, J. Up close with membrane lipid-protein complexes. *Science (80-.).* **334**, 320–321 (2011).
6. Browman, D. T., Hoegg, M. B. & Robbins, S. M. The SPFH domain-containing proteins: more than lipid raft markers. *Trends Cell Biol.* **17**, 394–402 (2007).
7. Tavernarakis, N., Driscoll, M. & Kyrpides, N. C. The SPFH domain: Implicated in regulating targeted protein turnover in stomatins and other membrane-associated proteins. *Trends Biochem. Sci.* **24**, 425–427 (1999).
8. Steglich, G., Neupert, W. & Langer, T. Prohibitins regulate membrane protein degradation by the m-AAA protease in mitochondria. *Mol. Cell. Biol.* **19**, 3435–3442 (1999).
9. Merkwirth, C. & Langer, T. Prohibitin function within mitochondria: Essential roles for cell proliferation and cristae morphogenesis. *Biochim. Biophys. Acta - Mol. Cell Res.* **1793**, 27–32 (2009).
10. Oyang, L. *et al.* The function of prohibitins in mitochondria and the clinical potentials. *Cancer Cell Int.* **22**, 1–10 (2022).
11. Merkwirth, C. *et al.* Prohibitins control cell proliferation and apoptosis by regulating OPA1-dependent cristae morphogenesis in mitochondria. *Genes Dev.* **22**, 476–488 (2008).
12. Da Cruz, S. *et al.* SLP-2 interacts with prohibitins in the mitochondrial inner membrane and contributes to their stability. *Biochim. Biophys. Acta - Mol. Cell Res.* **1783**, 904–911 (2008).
13. Christie, D. A. *et al.* Stomatin-Like Protein 2 Binds Cardiolipin and Regulates Mitochondrial Biogenesis and Function. *Mol. Cell. Biol.* **31**, 3845–3856 (2011).
14. Mitsopoulos, P. *et al.* Stomatin-Like Protein 2 Is Required for In Vivo Mitochondrial Respiratory Chain Supercomplex Formation and Optimal Cell Function . *Mol. Cell. Biol.* **35**, 1838–1847 (2015).
15. Nijtmans, L. G. J. *et al.* Prohibitins act as a membrane-bound chaperone for the stabilization of mitochondrial proteins. *EMBO J.* **19**, 2444–2451 (2000).
16. He, J. *et al.* Mitochondrial nucleoid interacting proteins support mitochondrial protein synthesis. *Nucleic Acids Res.* **40**, 6109–6121 (2012).
17. Mitsopoulos, P. *et al.* Stomatin-like protein 2 deficiency results in impaired mitochondrial translation. *PLoS One* **12**, 1–13 (2017).
18. Kihara, A., Akiyama, Y. & Ito, K. A protease complex in the Escherichia coli plasma membrane: HflKC (HflA) forms a complex with FtsH (HflB), regulating its proteolytic activity against SecY. *EMBO J.* **15**, 6122–6131 (1996).
19. Ma, C. *et al.* Structural insights into the membrane microdomain organization by SPFH family proteins. *Cell Res.* **32**, 176–189 (2022).
20. Osman, C., Merkwirth, C. & Langer, T. Prohibitins and the functional compartmentalization of mitochondrial membranes. *J. Cell Sci.* **122**, 3823–3830 (2009).
21. Wai, T. *et al.* The membrane scaffold SLP2 anchors a proteolytic hub in mitochondria containing PARL and the i -AAA protease YME1L . *EMBO Rep.* **17**, 1844–1856 (2016).
22. Matz, J. M., Goosmann, C., Matuschewski, K. & Kooij, T. W. A. An Unusual Prohibitin Regulates Malaria Parasite Mitochondrial Membrane Potential. *Cell Rep.* **23**, 756–767 (2018).
23. Artal-Sanz, M. & Tavernarakis, N. Prohibitin and mitochondrial biology. *Trends Endocrinol. Metab.* **20**, 394–401 (2009).
24. Esveld, S. L. Van *et al.* A Prioritized and Validated Resource of Mitochondrial Proteins in Plasmodium Identifies Unique Biology. *mSphere* **6**, e00614-21 (2021).
25. Saini, M. *et al.* Characterization of Plasmodium falciparum prohibitins as novel targets to block infection in humans by impairing the growth and transmission of the parasite. *Biochem. Pharmacol.* **212**, 115567 (2023).
26. Verhoef, J. M. J. *et al.* Detailing organelle division and segregation in Plasmodium falciparum *bioRxiv* 2024.01.30.577899 (2024).
27. Matz, J. M. *et al.* The Plasmodium berghei translocon of exported proteins reveals spatiotemporal dynamics of tubular extensions. *Sci. Rep.* **5**, 1–14 (2015).

28. Gehl, B. & Sweetlove, L. J. Mitochondrial Band-7 family proteins: Scaffolds for respiratory chain assembly? *Front. Plant Sci.* **5**, 1–6 (2014).
29. Heredia, M. Y. & Rauceo, J. M. The spfh protein superfamily in fungi: Impact on mitochondrial function and implications in virulence. *Microorganisms* **9**, (2021).
30. Tondera, D. *et al.* SlP-2 is required for stress-induced mitochondrial hyperfusion. *EMBO J.* **28**, 1589–1600 (2009).
31. Painter, H. J., Morrisey, J. M., Mather, M. W. & Vaidya, A. B. Specific role of mitochondrial electron transport in blood-stage Plasmodium falciparum. *Nature* **446**, 88–91 (2007).
32. MacRae, J. I. *et al.* Mitochondrial metabolism of sexual and asexual blood stages of the malaria parasite Plasmodium falciparum. *BMC Biol.* **11**, (2013).
33. Evers, F. *et al.* Composition and stage dynamics of mitochondrial complexes in Plasmodium falciparum. *Nat. Commun.* **12**, 3820 (2021).
34. Zhang, M. *et al.* Uncovering the essential genes of the human malaria parasite Plasmodium falciparum by saturation mutagenesis. *Science* **360**, eaap7847 (2018).
35. Toenhake, C. G. *et al.* Chromatin Accessibility-Based Characterization of the Gene Regulatory Network Underlying Plasmodium falciparum Blood-Stage Development. *Cell Host Microbe* **23**, 557-569.e9 (2018).
36. Tanveer, A. *et al.* An FtsH protease is recruited to the mitochondrion of Plasmodium falciparum. *PLoS One* **8**, e74408 (2013).
37. Merkwirth, C. & Langer, T. Prohibitin function within mitochondria: essential roles for cell proliferation and cristae morphogenesis. *Biochim. Biophys. Acta* **1793**, 27–32 (2009).
38. Shi, H., Rampello, A. J. & Glynn, S. E. Engineered AAA+ proteases reveal principles of proteolysis at the mitochondrial inner membrane. *Nat. Commun.* **7**, 1–12 (2016).
39. Serricchio, M. & Bütikofer, P. A Conserved Mitochondrial Chaperone-Protease Complex Involved in Protein Homeostasis. *Front. Mol. Biosci.* **8**, 767088 (2021).
40. Jumper, J. *et al.* Highly accurate protein structure prediction with AlphaFold. *Nature* **596**, 583–589 (2021).
41. Evans, R. *et al.* Protein complex prediction with AlphaFold-Multimer. *BioRxiv* (2022) doi:10.1101/2021.10.04.463034v1.
42. Sparkes, P. C. *et al.* Mitochondrial ATP synthesis is essential for efficient gametogenesis in Plasmodium falciparum. *bioRxiv* (2024).
43. Boucher, M. J. *et al.* Integrative proteomics and bioinformatic prediction enable a high-confidence apicoplast proteome in malaria parasites. *PLoS Biol.* **16**, 1–29 (2018).
44. Nguyen, T. T. & Voeltz, G. K. An ER phospholipid hydrolase drives ER-associated mitochondrial constriction for fission and fusion. *Elife* **11**, 1–30 (2022).
45. Leonhard, K. *et al.* Membrane protein degradation by AAA proteases in mitochondria: Extraction of substrates from either membrane surface. *Mol. Cell* **5**, 629–638 (2000).
46. Gerdes, F., Tatsuta, T. & Langer, T. Mitochondrial AAA proteases - Towards a molecular understanding of membrane-bound proteolytic machines. *Biochim. Biophys. Acta - Mol. Cell Res.* **1823**, 49–55 (2012).
47. Amberg-Johnson, K. *et al.* Small molecule inhibition of apicomplexan FtsH1 disrupts plastid biogenesis in human pathogens. *Elife* **6**, (2017).
48. Karnataki, A., Derocher, A. E., Coppens, I., Feagin, J. E. & Parsons, M. A membrane protease is targeted to the relict plastid of toxoplasma via an internal signal sequence. *Traffic* **8**, 1543–1553 (2007).
49. Song, Z., Chen, H., Fiket, M., Alexander, C. & Chan, D. C. OPA1 processing controls mitochondrial fusion and is regulated by mRNA splicing, membrane potential, and Yme1L. *J. Cell Biol.* **178**, 749–755 (2007).
50. Guillery, O. *et al.* Metalloprotease-mediated OPA1 processing is modulated by the mitochondrial membrane potential. *Biol. Cell* **100**, 315–325 (2008).
51. Marques, I., Dencher, N. A., Videira, A. & Krause, F. Supramolecular organization of the respiratory chain in Neurospora crassa mitochondria. *Eukaryot. Cell* **6**, 2391–2405 (2007).
52. Ma, C. *et al.* Structural insights into the membrane microdomain organization by SPFH family proteins. *Cell Res.* **32**, 176–189 (2022).
53. Deitsch, K. W., Driskill, C. L. & Wellems, T. E. Transformation of malaria parasites by the spontaneous uptake and expression of DNA from human erythrocytes. *Nucleic Acids Res.* **29**, 850–853 (2001).
54. Ponnudurai, T., Lensen, A. H. W., Meis, J. F. G. M. & Meuwissen, J. H. E. Synchronization of Plasmodium falciparum gametocytes using an automated suspension culture system. *Parasitology* **93**, 263–274 (1986).
55. Rappsilber, J., Ishihama, Y. & Mann, M. Stop And Go Extraction tips for matrix-assisted laser

desorption/ionization, nanoelectrospray, and LC/MS sample pretreatment in proteomics. *Anal. Chem.* **75**, 663–670 (2003).

56. Cox, J. & Mann, M. MaxQuant enables high peptide identification rates, individualized p.p.b.-range mass accuracies and proteome-wide protein quantification. *Nat. Biotechnol.* **26**, 1367–1372 (2008).

57. PlasmoDB: An integrative database of the Plasmodium falciparum genome. Tools for accessing and analyzing finished and unfinished sequence data. The Plasmodium Genome Database Collaborative. *Nucleic Acids Res.* **29**, 66–69 (2001).

58. Tyanova, S. *et al.* The Perseus computational platform for comprehensive analysis of (prote)omics data. *Nat. Methods* **13**, 731–740 (2016).

59. Schalkwijk, J. *et al.* Antimalarial pantothenamide metabolites target acetyl-coenzyme A biosynthesis in Plasmodium falciparum. *Sci. Transl. Med.* **11**, (2019).